Journal of Biomolecular NMR, **13:** 233–247, 1999.
KLUWER/ESCOM

High resolution solution structure of apo calcyclin and structural variations in the S100 family of calcium-binding proteins

Lena Mäler, Barbara C.M. Potts & Walter J. Chazin*
Department of Molecular Biology (MB9), The Scripps Research Institute, 10550 North Torrey Pines Road, La Jolla, CA 92037, U.S.A.

Received 21 September 1998; Accepted 18 November 1998

Key words: calcium-binding protein, calcyclin, protein structure, S100 protein

Abstract

The three-dimensional solution structure of apo rabbit lung calcyclin has been refined to high resolution through the use of heteronuclear NMR spectroscopy and ^{13}C,^{15}N-enriched protein. Upon completing the assignment of virtually all of the ^{15}N, ^{13}C and ^{1}H NMR resonances, the solution structure was determined from a combination of 2814 NOE-derived distance constraints, and 272 torsion angle constraints derived from scalar couplings. A large number of critical inter-subunit NOEs (386) were identified from ^{13}C-select,^{13}C-filtered NOESY experiments, providing a highly accurate dimer interface. The combination of distance geometry and restrained molecular dynamics calculations yielded structures with excellent agreement with the experimental data and high precision (rmsd from the mean for the backbone atoms in the eight helices: 0.33 Å). Calcyclin exhibits a symmetric dimeric fold of two identical 90 amino acid subunits, characteristic of the S100 subfamily of EF-hand Ca^{2+}-binding proteins. The structure reveals a readily identified pair of putative sites for binding of Zn^{2+}. In order to accurately determine the structural features that differentiate the various S100 proteins, distance difference matrices and contact maps were calculated for the NMR structural ensembles of apo calcyclin and rat and bovine S100B. These data show that the most significant variations among the structures are in the positioning of helix III and in loops, the regions with least sequence similarity. Inter-helical angles and distance differences for the proteins show that the positioning of helix III of calcyclin is most similar to that of bovine S100B, but that the helix interfaces are more closely packed in calcyclin than in either S100B structure. Surprisingly large differences were found in the positioning of helix III in the two S100B structures, despite there being only four non-identical residues, suggesting that one or both of the S100B structures requires further refinement.

Abbreviations: NOE, nuclear Overhauser enhancement; CaBP; Ca^{2+}-binding protein; rMD, restrained molecular dynamics; rmsd, root mean square deviation.

Introduction

Calcyclin is a member of the S100 subfamily of EF-hand Ca^{2+}-binding proteins (CaBPs). EF-hand proteins have been widely implicated in intracellular Ca^{2+}-dependent signal transduction pathways, both as sensors and modulators of the ionic signal. The S100s are purported to have sensor roles that may mimic signaling pathways of the ubiquitous Ca^{2+}-regulator calmodulin, but in a highly specific cell-type manner. S100 proteins have been implicated in the control of cell growth and differentiation, energy metabolism, and cytoskeletal-driven changes in cell shape (reviewed in Donato, 1991; Schäfer and Heizmann, 1996). These proteins also exhibit the unique property of deregulated expression in association with human disease. Specific S100 proteins have been linked to neurological disorders, including Alzheimer's disease, Down's syndrome, and epilepsy, to inflammatory disorders such as cystic fibrosis, arthritis and bronchitis,

*To whom correspondence should be addressed. E-mail: chazin@scripps.edu

and to cancers (van Heyningen et al., 1985; Roth et al., 1992; Brun et al., 1994; Ilg et al., 1996; Schäfer and Heizmann, 1996). Most of the S100 genes are found in the 1q21 region of human chromosome 1, a region that frequently displays alterations upon tumor transformation (Engelkamp et al., 1993).

Calcyclin is one of the genes in the 1q21 cluster that displays deregulated expression in transformed cells. More specifically, calcyclin has been shown to be upregulated in the cells of patients with acute myeloid leukemia and in certain breast cancer and melanoma cell lines (Calabretta et al., 1985, 1986; Murphy et al., 1988). The calcyclin 2A9 gene was originally identified as a cell-cycle dependent gene that displayed increased expression in G_1. Calcyclin has been shown to bind glyceraldehyde-3-phosphate dehydrogenase, sialic acid, a novel 30 kDa protein from Ehrlich ascites tumor cells, and like many other S100 proteins, a specific annexin protein (annexin XI) (Zeng and Gabius, 1991; Minami et al., 1992; Zeng et al., 1993; Filepek and Kuznicki, 1998). The annexins are protein kinase substrates that exhibit Ca^{2+}-dependent binding to phospholipids, consistent with a role in cytoskeletal-related functions. The highly specific Ca^{2+}-dependent interaction of calcyclin with the regulatory domain of annexin XI suggests a role for the protein in modulating the phosphorylation state of the annexin and thereby regulating its association with the cellular membrane. The localization of annexin XI to the nuclei of certain cells and concentration around the mitotic apparatus during M phase implicate this system in the regulation of cell growth or division.

As part of the effort to understand the functional properties and cellular activities of calcyclin, we have undertaken detailed biophysical and structural characterization of this protein and its interaction with putative targets. The low-resolution structure of native rabbit lung calcyclin in the absence of Ca^{2+} revealed a striking structural similarity between the apo calcyclin dimer subunit and the ancestral S100 protein, calbindin D_{9k}, which exists in solution as a monomer (Potts et al., 1996). The structure of recombinant rabbit calcyclin in the Ca^{2+}-loaded state confirmed that the mode of binding to target proteins by the S100 subfamily is fundamentally different than those of calmodulin and troponin C, the prototypical Ca^{2+} sensors (Sastry et al., 1998). In this report, we describe the highly refined NMR solution structure of apo recombinant rabbit calcyclin. The structural differences between apo and Ca^{2+}-bound calcyclin seem to be very modest (Potts et al., 1995; Sastry et al., 1998), therefore very high-resolution structures are necessary to understand the Ca^{2+}-induced structural changes that are central to the biological function of this protein. In addition, we are able to propose the location and ligation pattern for the previously characterized Zn^{2+} binding site.

The three-dimensional (3D) structure of a second S100 protein, S100B, has also been reported, both in the absence and presence of Ca^{2+} (Drohat et al., 1996, 1998; Kilby et al., 1996; Matsumura et al., 1998; Smith and Shaw, 1998). In addition, the three-dimensional structure of psoriasin, a third homolog, with bound holmium has recently been reported (Brodersen et al., 1998). All of these structures exhibit the same distribution of structural elements and global fold as calcyclin, although they clearly vary in detail. While there are multiple S100B structures, and the nature of Ca^{2+}-dependent changes is most clearly defined for this protein, structures in both the absence and presence of Ca^{2+} have been determined only for S100B from rat. The bovine and human proteins differ from the rat protein by only four and two substitutions, respectively, with only one being non-conservative. However, the extent of differences between the structures of bovine and rat S100B in the absence of Ca^{2+} is far larger than what is expected on the basis of their respective precisions. In the interest of obtaining insights into this apparent anomaly, as well as examining the structural variations within this group of proteins, we have compared the two apo S100B structures to each other and to our very high resolution solution NMR structure of apo calcyclin.

Materials and methods

Creation of the expression system, over-expression and purification of labeled recombinant rabbit calcyclin have been described elsewhere (Sastry et al., 1998). The samples used for collecting the NMR data were all at a protein concentration of 1–2 mM and in a buffer containing 50 mM Tris-d_{11} at pH 7.0. Samples with ^{15}N or ^{15}N,^{13}C-enriched protein contained 0.05% NaN_3. Five samples were prepared: (1) uniformly ^{15}N,^{13}C-enriched; (2) uniformly ^{15}N-enriched; (3) 10% ^{13}C-enriched; (4) unlabeled; (5) a 1:1 mixture of uniformly ^{15}N,^{13}C-enriched and unlabeled protein. The mixing of labeled and unlabeled protein was carried out at room temperature and monitored by mass spectrometry. Mass peaks corresponding to unlabeled, asymmetrically labeled and fully labeled protein could

be detected and after two days the 1:2:1 equilibrium was reached. Experiments were either carried out in D_2O or in H_2O with ~25 μl D_2O for field/frequency lock stabilization.

NMR spectroscopy

The NMR experiments were performed at 300 K using Bruker AMX600 and DMX750 spectrometers equipped with triple-resonance probe heads and pulsed field gradients. A relaxation delay of about 1 s was employed prior to acquisition, except for the NOESY experiments where a delay of 1.5–2 s was used. Quadrature detection was achieved by the States-TPPI method (Marion et al., 1989a). The spectra were processed and analyzed using the FELIX software (version 95.0, MSI, San Diego, CA). Processing involved extending the FIDs in the indirectly detected dimensions by linear predicting approximately 25% additional points. FELIX was also used for assistance in making the spectral frequency assignments, and for bookkeeping.

Triple-resonance experiments were typically recorded with 256 (direct ^{1}H), 50 (^{15}N), 40 (^{13}C) complex points in the three dimensions, using standard pulse sequences (Cavanagh et al., 1996) with extensive use of field gradients. The data were subsequently linear predicted, zero-filled, and Fourier transformed to obtain 256 × 256 × 128 matrices for cross peak analysis. Side-chain amide ^{15}N and ^{1}H chemical shifts were obtained from a ^{15}N-^{1}H HSQC. Stereospecific assignments of Leu and Val methyl resonances were obtained from a ^{13}C-^{1}H HSQC spectrum recorded on the 10% ^{13}C-labeled sample.

Several different NOESY experiments (Jeener et al., 1979) were recorded. For the unlabeled sample, 2D ^{1}H NOESY spectra were recorded with mixing times of 60 ms and 18 ms. A NOESY spectrum with a mixing time of 200 ms was recorded on the unlabeled sample in D_2O. A 2D NOESY experiment (τ_{mix} = 60 ms) was obtained for the ^{15}N-labeled sample without ^{15}N-decoupling during acquisition. All but the latter experiment were recorded with a Hahn-echo appended for improving the baseline. Each homonuclear ^{1}H spectrum was acquired with 512 t_1 increments. A 3D ^{13}C NOESY-HSQC spectrum (Marion et al., 1989b) and a 4D ^{13}C,^{13}C HMQC-NOESY-HMQC (Vuister et al., 1993) spectrum were recorded with the double-labeled sample. The mixing time for these spectra was 100 ms. The 3D spectrum was acquired with 256, 98, 128 complex points in the direct ^{1}H, ^{13}C and indirect ^{1}H dimensions respectively, and the processed data were zero-filled to a matrix size of 256 × 256 × 256 complex points. The 4D data set was recorded on a sample in D_2O with 256 (direct ^{1}H), 18 (^{13}C), 40 (indirect ^{1}H), 18 (^{13}C) complex points. Linear prediction in both ^{13}C-dimensions and zero-filling yielded a final processed matrix size of 256 × 64 × 128 × 64 complex points. The 1:1 mixture of labeled and unlabeled protein was used to collect 2D (τ_{mix} = 100 ms) and 3D (τ_{mix} = 115 ms) ^{13}C-edited,^{13}C-filtered NOESY experiments (Lee et al., 1994). The 3D spectrum was acquired with 512 points in the direct ^{1}H dimension, 48 in the ^{13}C and 96 in the indirect ^{1}H dimension and the final processed matrix size was linear predicted/zero-filled to 512 × 128 × 256 complex points. Two additional experiments were acquired for coupling constant measurements. A 3D HNHA experiment (Vuister and Bax, 1993) was recorded on ^{15}N-labeled protein with 512×50×63 complex points, and the final processed matrix was linear predicted and zero-filled to 512 × 128 × 128 points. A 3D HACAHB-COSY (Grzesiek et al., 1995) was recorded with double-labeled protein in D_2O with 256×55×80 complex points, and the final processed matrix was linear predicted and zero-filled to 256 × 256 × 256.

Input constraints

Distance constraints were generated from integrated cross-peak volumes in the 3D NOESY-HSQC, 4D HMQC-NOESY-HMQC and 2D homonuclear NOESY spectra. The 3D and 4D ^{13}C-edited experiments provided the bulk of all NOE contacts. The 2D ^{1}H NOESY (τ_{mix} = 60 ms) was used for NOEs between amide protons and the 2D NOESY (τ_{mix} = 200 ms) recorded in D_2O was used for the aromatic-aromatic NOEs. Automated assignments of NOEs based only on chemical shifts were made by using the program GENXPK (Gippert, 1995). Assignments of cross peaks that are degenerate in chemical shift in one or several dimensions were made using a filtering strategy based on the distances in the most recent round of calculated structures. The constraints derived from NOE volumes were given upper distance bounds of 4.2, 5.2 and 6.0 Å (3D), 4.5 and 6.0 Å (4D), 3.4, 4.0 and 6.0 Å (2D) and an upper bound of 6.0 Å for the NOESY recorded in D_2O. Pseudo-atom corrections were included as described by Wüthrich et al. (1983). The upper distance bounds were set by the following procedures. First, an internal calibration was made based on the volumes of characteristic sequential and medium-range NOEs for residues within ordered structural elements and from

intra-residue NOEs. These bounds were refined just before the final round of structure calculations by carrying out a series of calculations in which the upper distance bounds were systematically varied. The appropriateness of the applied bounds was then judged by examining the molecular energies, rmsd values and distance constraint violations for each family of structures. When the empirical upper bounds were loosened, the only effect was a slight increase in rmsd. The upper bounds were then tightened until either constraint violations or molecular energies started to differ from the values in the initial conformational ensemble. The values for the final tighter bounds did not differ from the initial values by more than 0.3 Å. Distance constraints from the ^{13}C-edited, ^{13}C-filtered experiments were obtained in a similar way, starting from an internal calibration scheme and the constraints were given upper distance bounds of 4.2, 5.2 and 6.0 Å. Twelve hydrogen bonds were included in the distance geometry calculations only. These were assigned based on their slow exchange and characteristic NOEs for α-helical or β-type anti-parallel conformation and implemented as described previously (Potts et al., 1996).

Torsion angle constraints were obtained from analyzing the HNHA and HACAHB-COSY experiments in combination with NOEs obtained from a short mixing time NOESY (18 ms). Values for $^{3}J_{HN\alpha}$ were calculated from cross-peak volume ratios in the 3D HNHA experiment. The minimum ranges used for ϕ angles were $\pm 25°$. Side-chain χ_1 torsion angles and stereospecific assignments of β-methylene groups were obtained from $^{3}J_{\alpha\beta}$ in combination with H^N-H^β and H^α-H^β NOEs. The values of $^{3}J_{\alpha\beta}$ were obtained by taking the ratio of cross-peak and diagonal-peak intensities in the HACAHB-COSY as described by Grzesiek et al. (1995). χ_1 angles were given a range of $\pm 40°$. Stereospecific assignments of the prochiral isopropyl methyl groups in Val and Leu residues were made based on cross-peak patterns observed in a ^{13}C-^{1}H HSQC spectrum acquired from the 10% ^{13}C-labeled sample (Senn et al., 1989). The C^β protons of Pro4 were assigned on the basis of intra-residue NOE intensities (Kline et al., 1988). A few additional stereospecific assignments were subsequently made by a statistical analysis of families of structures.

Structure calculation

The initial stage of structure calculations involved the generation of 50 subunit structures using the program DIANA (Güntert et al., 1991) together with the REDAC strategy (Güntert and Wüthrich, 1991). These starting structures were then refined using the SANDER module of AMBER (version 4.1; Pearlman et al., 1995). The rMD protocol consisted of 3000 steps of minimization prior to a 10 ps restrained molecular dynamics annealing cycle as previously described (Potts et al., 1995). The first dimer starting structure was generated by positioning two copies of one subunit structure ∼80 Å apart using NAB (Macke, 1996). Additional structures were then generated by systematically varying the relative orientation, resulting in 48 dimer starting structures. The distance of separation between the two subunits was optimized by trial and error until the highest rate of convergence for docking was achieved. Dimer structures were generated from three different subunit starting structures to ensure that the final dimer structures were not biased by the choice of starting structure. The dimer starting structures were docked by rMD over 25 ps, during which the inter-molecular subunit restraints were ramped on from a force constant of 0 kcal mol^{-1} Å^{-2} to 32 kcal mol^{-1} Å^{-2}. All restraints within the subunits were maintained with force constants of 32 kcal mol^{-1} Å^{-2} throughout the simulation. The resulting dimer structures were subsequently refined by a 20 ps annealing cycle. The program FindFam (Smith et al., 1996) was used to determine that 22 structures were needed to accurately represent the family of structures. The 96 converged dimer structures were then ordered by experimental constraint violation energies and the top 22 structures were chosen based on their constraint and total molecular energies. The coordinates of the final structures together with the input constraint list are deposited with the Brookhaven Protein Data Bank under accession code 2CNP.

Structure analysis

Molecular structures were displayed and graphically analyzed using Insight II (version 97.0, MSI, San Diego, CA). The family of final structures was analyzed using the PROCHECK NMR software (Laskowski et al., 1993). Angle, NOE and torsion violations, as well as hydrogen bonds were analyzed with the aid of the programs distributed with the GAP software package (NOEVIO, TORVIO, HBONDS and ANGLES; http://www.fkem2.lth.se/∼garry/programs.html). Super-positioning of structures to obtain root mean square deviations for the family of structures as well as comparisons with other structures were done with the program suppose (http://www.scripps.edu/∼jsmith/suppose). Inter-helical angles were mea-

sured using the software provided by Stéphane M. Gagné (University of Alberta, Edmonton, AB). Distance difference matrices were calculated with the DISCOM program and analyzed with in-house written scripts to convert the distance differences to visual constraints that could be displayed using Insight II. Inter-residue contacts were calculated with CHARMM as described elsewhere (Nelson and Chazin, 1998), and in-house scripts were used to analyze the results.

Results

Heteronuclear and stereospecific assignments

The heteronuclear chemical shift assignments were obtained from a combination of triple-resonance and ^{13}C-edited experiments, including HNCA, CBCA(CO)NH, HCCH-COSY and HCCH-TOCSY. A large number of proton chemical shift assignments were previously reported (Potts et al., 1996) and these greatly facilitated making the heteronuclear assignments. (Seven previously assigned proton resonances were found to be incorrect, but of these, four had only been assigned tentatively before. The three incorrect assignments were found for Met0 C^{β}-methylene protons and for one of the Leu11 C^{δ}-methyl groups.) Virtually all of the backbone ^{15}N and C^{α} chemical shifts could be identified in the HNCA experiment. The assignments were confirmed and extended to C^{β} from the analysis of the CBCA(CO)NH experiment. The carbon assignments were further extended to side chains by the HCCH-COSY and HCCH-TOCSY data. These spectra enabled virtually complete ^{1}H chemical shift assignments for the side chains, which was not possible based on homonuclear ^{1}H data alone. In the end, all backbone ^{15}N and $^{13}C^{\alpha}$ assignments could be made with the exception of the amide ^{15}N frequencies of Ser20 and Ser46. All side chain carbons were assigned except for residue Lys31. All of the methyl groups in Leu and Val residues were stereospecifically assigned by examining the labeling patterns in the ^{13}C-^{1}H HSQC experiment recorded on a partially ^{13}C-labeled sample as described by Senn et al. (1989). Stereospecific assignments of C^{β}-methylene protons were obtained from a combination of the $^{3}J_{\alpha\beta}$ coupling constants and intra-residue NOEs. Assignments were only made when all experimental evidence unambiguously showed one possible assignment as well as one conformation around the C^{α}-C^{β} bond. Additional C^{β}-methylene stereospecific assignments were made for Tyr84 and Leu88 at a later stage, based on structural statistics in combination with careful inspection of intra-residue NOEs. These assignments as well as additional χ_1 angle restraints were only used in the last stages of the structure calculation. In all, 29 of the 51 potential stereospecific C^{β} proton assignments were obtained.

Assignments of inter-molecular NOE contacts

In order to obtain the most accurate and precise structure possible, the assignment of the maximum number of inter-subunit NOEs was imperative. It was previously determined that the dimer interface is primarily defined by a four-helix bundle consisting of helices I, I′, IV and IV′. Due to the symmetry of the dimer interface, many of the inter-molecular NOEs are almost impossible to distinguish from intra-molecular NOEs. It was therefore not possible to obtain many unambiguous NOE contacts from the regular homonuclear or ^{13}C-edited NOESY experiments. To this end, 2D and 3D ^{13}C-edited, ^{13}C-filtered NOESY experiments (Lee et al., 1994) were recorded on a 1:1 mixture of labeled and unlabeled proteins to identify NOEs solely between one proton on the labeled subunit and a second on the unlabeled subunit, i.e. across the dimer interface. Figure 1 shows strips from the 3D experiment to demonstrate the quality of the data.

Initially, we were able to assign ∼70 NOEs originating from each subunit (corresponding to a total of 140 distance constraints for the dimer) based on the uniqueness of chemical shifts alone, and these were used to calculate the first set of dimer structures. This allowed us to use distance filtering against the best available structures to assign additional inter-molecular NOEs in the other NOESY experiments as described in Sastry et al. (1998). All inter-molecular NOEs initially suggested in this way were subsequently confirmed in either the 3D or 2D select-filtered experiment. Due to the relatively high sensitivity, three different 2D versions of the experiment were recorded, optimized for ω_1\{aliphatic\}-ω_3\{aliphatic\}, ω_1\{aliphatic\}-ω_3\{aromatic\} and ω_1\{aromatic\}-ω_3\{aromatic\} carbons, respectively. The spectra involving aromatic carbons were of much poorer quality and only a few such inter-molecular NOEs could be directly detected. The inter-molecular aromatic-aliphatic NOEs were mainly obtained from the 3D ^{13}C NOESY-HSQC. Aromatic-aromatic contacts were obtained from the 2D NOESY in D_2O. These NOEs were only used if intra-molecular assignments could be ruled out from examining the

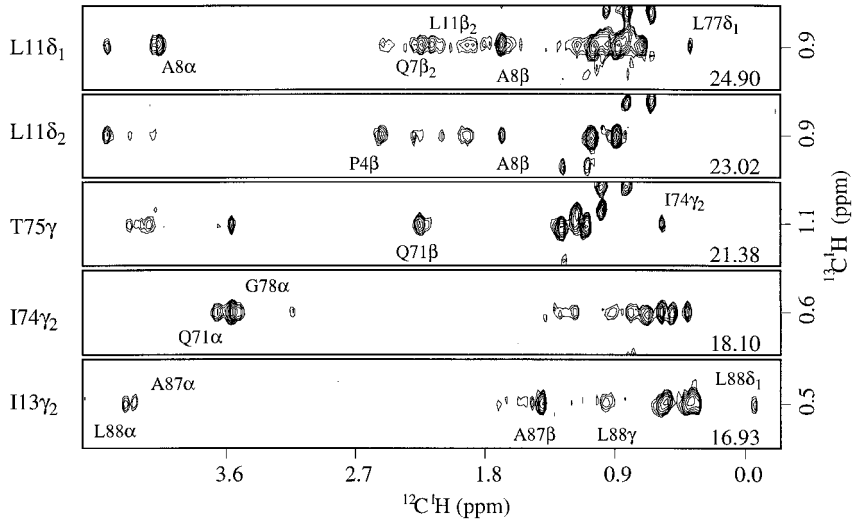

Figure 1. Selected 2D strips at different ^{13}C-frequencies from the 3D ^{13}C select-^{13}C filtered NOESY experiment on apo calcyclin at pH 7 and 27 °C. The identity of cross peaks that can be unambiguously assigned on the basis of chemical shifts alone is indicated. The experiment was recorded on a mixed 1:1 ^{13}C,^{15}N-labeled/unlabeled protein in D_2O.

calculated structures. At later stages in the calculations, NOEs that were judged feasible as both intra- and inter-molecular contacts were included, but were given a conservative upper distance limit of 6 Å. In the final round of structure calculation, a total of 386 inter-molecular NOEs were used. The NOE contacts primarily involve helices I, I′, IV and IV′ and among these especially residues Pro4, Leu5, Leu11, Ile13, Phe16, Phe70, Tyr73, as well as Leu88 seem to be important in defining the dimer interface. There are however a few NOEs between helix I and the linker region of the other subunit, as well as other NOEs involving His27 and Leu48.

Quality and precision of structures

In the structure refinement of apo calcyclin, a total of 2814 NOE-derived distance constraints were incorporated as well as 272 experimentally derived torsion angle constraints. Figure 2 shows the number of distance constraints per residue and the calculated pairwise rmsd per residue. The number of constraints is almost three times as large as what was used in the previous low-resolution structure calculation, due to the ability to obtain near complete and unambiguous resonance and NOE assignments from the heteronuclear NMR experiments. Furthermore, the number of inter-molecular NOEs has increased from 52 to 386 as a byproduct of acquiring filter-edited NOESY experiments on a mixture of labeled and unlabeled protein.

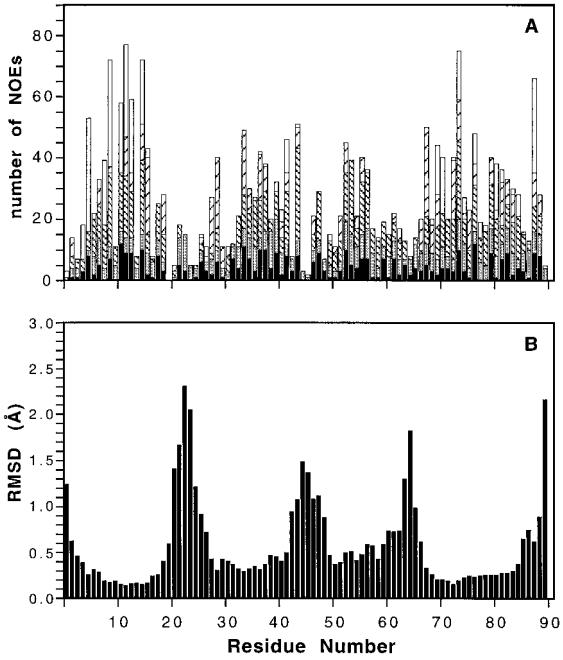

Figure 2. Plots of per residue NOE-derived distance constraints (A) and per residue rmsd from the mean (B) for apo calcyclin. All inter-residue constraints in (A) appear twice. The constraints are grouped into four categories: intra-residue (filled), sequential (dotted), medium-range (hatched) and long-range ($|i - j| \geq 5$, wide hatched) and inter-molecular (open).

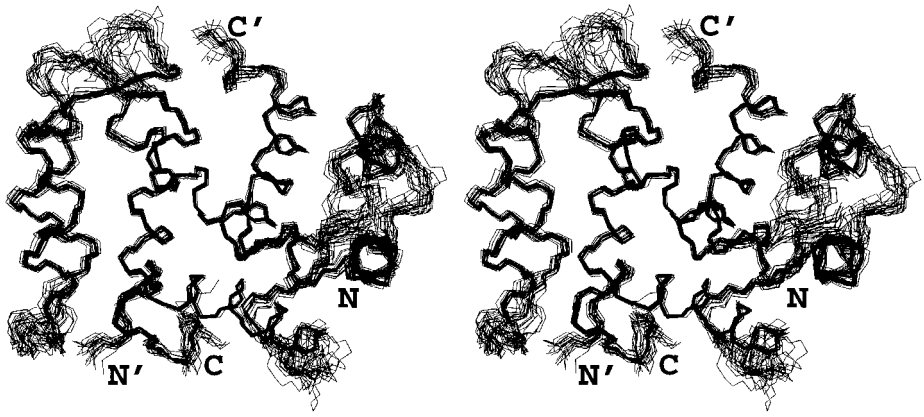

Figure 3. Stereoview of the ensemble of 22 apo calcyclin structures. The conformers were superimposed using all heavy atoms.

Consequently, an entirely new structure was calculated based on the new constraints.

The procedure for the structure calculation followed closely the outlined methods used in the previous structure determinations of calcyclin (Potts et al., 1995). A few differences are worth pointing out. Due to the high number of inter-molecular NOEs, it was necessary to modify the docking procedure slightly, increasing the separation of the two subunits at the start of docking from 40 Å to 80 Å. This increase in separation was based on a series of experiments in which the distance between the two subunits was varied from 40 to 100 Å. Although the previously noted problems with convergence were mostly overcome,we observed that for certain starting geometries the subunits never docked in a proper manner. For the final round of calculations, 18 of the 114 starting dimer structures were discarded as it was clear that docking of the two subunits was unsuccessful. These 18 structures all exhibited very large constraint violations and an asymmetric fold, inconsistent with the experimental data.

A final ensemble of 22 structures was selected to represent the apo calcyclin structure. Figure 3 shows a stereo-view of the ensemble after superpositioning over all heavy atoms. This family of structures has very small constraint violation energies, no distance constraint violation larger than 0.15 Å, no torsion angle violation greater than 4.4° and low molecular energies (Table 1). Furthermore, the precision of the ensemble was high, reflected for example by the backbone rmsd from the mean for all ordered structural elements of 0.33 Å. Moreover, the rmsd for all backbone atoms in the dimer is comparable to that of the subunits, revealing that the dimer interface is very well defined (Table 1). The difference between any pair of the subunits is very small, indicating that the complex is highly symmetric, even though no explicit symmetry constraints were imposed during the calculation. The eight helices in the structure are the most well defined. The Ca^{2+}-binding loops and the linker region between the two EF-hands are less well defined, with Ca^{2+}-binding loop I being the least well-determined part of the structure.

The PROCHECK NMR program was used to further assay the quality of the structure. The analysis of backbone dihedral angles ϕ and ψ shows that 98% of all non-glycine residues fall within the favorable regions of conformational space: 80% in the most favored, 18% in the allowed and less than 1% in the generously allowed regions. Among all of the structures, only 1.5% of the residues fall outside the allowed regions, and no residue falls consistently outside the allowed regions. Moreover, the residues that do fall outside the allowed regions are all in the least well-defined regions of the structure (residues Ala2, Ser3, Tyr19–Lys26, Ile44–Asp50, Asn63–Glu67). In Figure 4, the mean values of the ϕ, ψ and χ_1 dihedral angles are shown together with their respective standard deviation. The backbone angles for the helices and short β-strands show well-defined values with low standard deviations. Most of the χ_1 angles adopt one of the three possible rotamer states. For certain residues, the side chains are seen to occupy a wide range of conformations, a reflection of the absence of specific experimental constraints.

Description of the structure

As previously reported, calcyclin adopts the homodimeric fold which appears to be the general structural

Table 1. Structural statistics for the ensembe of 22 dimer structures

Constraint violations, mean and standard deviation	
Distance (Å)	
$0.1 \leq d < 0.2$	0.5 ± 0.7
$0.2 \leq d$	0
$0 \leq d$	114 ± 6
Average maximum violation	0.10 ± 0.02
Average total violation	0.025 ± 0.001
Torsion (°)	
$\theta \leq 5.0$	11 ± 3
$5.0 < \theta$	0
Average maximum violation	3.1 ± 0.9
Average total violation	1.3 ± 0.4
AMBER energies, mean and standard deviation (kcal mol^{-1})	
Constraint energy	5.0 ± 0.4
Lennard-Jones	-1098 ± 10
Total	-2675 ± 17
Root mean square deviations (Å)	
Average pairwise from mean structure, all atoms	1.16
all backbone	0.73
backbone in helices[a] (dimer, subunit)	0.33, 0.30

[a]Helices are defined as: I (4–18); II (31–41); III (50–62); IV (70–84). Dimer rmsd after fitting over all eight helices. Subunit rmsd after fitting the four helices of each subunit independently.

paradigm for S100 proteins (Potts et al., 1995). Each subunit consists of the four-helix bundle comprising two EF-hands. The two EF-hands are connected by an eight-residue linker. The beginning and end of the four helices were identified as described by Kördel et al. (1993), based on a combination of (i, i + 3) and (i, i + 4) hydrogen bonds and backbone dihedral angles. Helix I extends from Ser3 to Lys18 with a standard (i, i + 4) α-helical hydrogen bonding pattern, but with the ψ backbone dihedral angle of Ser3 outside of the helical range. There is an indication of an N-cap hydrogen bond from Asp6 HN to Ser3 O^{γ}, although it is found in only 6 out of the 22 structures. Helix II starts at Lys31 and ends with Leu42, with a purely α-helical hydrogen bonding pattern. Again, there is some indication of an N-cap hydrogen bond in this helix between Glu33 HN and Ser30 O^{γ}, but the N-cap is formally present in only two structures. The third helix starts at Asp50 and extends to Asn63. The middle of helix III is slightly irregular, as the Met57 main-chain O forms a 3_{10}-helical (i, i + 3) hydrogen bond with Leu60 NH. Moreover, the Leu56 main-chain O is not involved in a helical hydrogen bond, and Asp61 NH hydrogen bonds to Asp58 main-chain O in six of the structures. The Asp58 main-chain O is also fully hydrogen bonded in the normal α-helical manner to Arg62 NH. A regular α-helical hydrogen bonding pattern in helix IV is observed, which extends from Asn69 to Asn85. Asn69 is also involved in the short β-type interaction defined for residues 67–69. This residue is highly analogous to the homologous residue in calbindin D_{9k}, in that it participates in both elements of secondary structure, fulfilling the hydrogen bonding requirement at the N-terminus of helix IV, while occupying backbone dihedral angles clearly in the β-region of (ϕ,ψ)-space. The helix is capped at its N-terminus by a hydrogen bond from Glu72 HN to Asn69 $O^{\delta 1}$, which is present in 70% of the structures.

The two Ca^{2+}-binding loops are situated on the same side of the protein between helices I and II and between helices III and IV and they are connected by an antiparallel β-type interaction involving Thr28–Ser30 and Glu67–Asn69. The expected hydrogen bonds between Leu29 and Val68 are present in all 22 structures and all backbone dihedral angles are in the β-region of (ϕ,ψ) space. The N-terminal regions of both Ca^{2+}-binding loops are ill-defined with loop I being less defined than loop II. This could indicate that

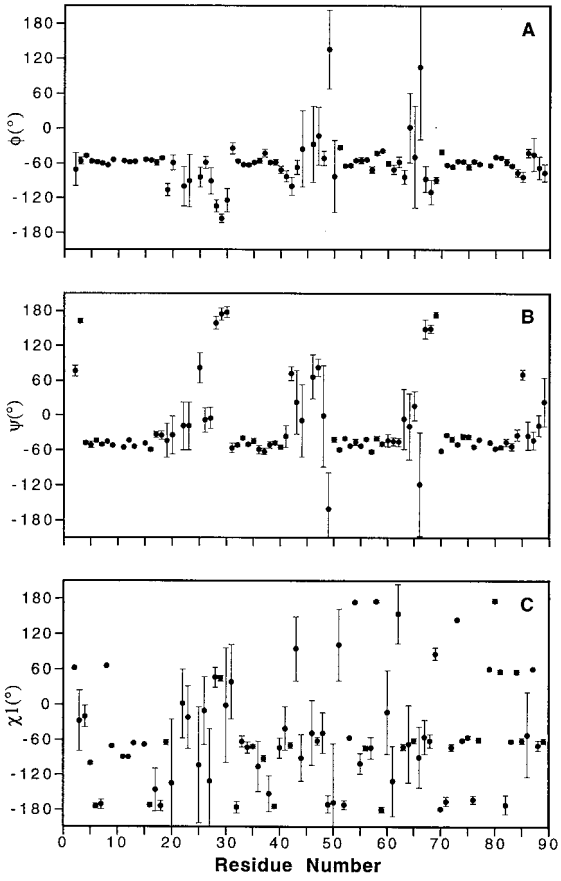

Figure 4. The ϕ (A), ψ (B) and χ_1 (C) torsion angles observed in the ensemble of 22 apo calcyclin structures. The mean for each residue is displayed together with the standard deviation.

the first loop is more flexible, an observation which is further supported by preliminary ^{15}N relaxation data (O. Crescenzi and W.J. Chazin, unpublished results). This would however constitute a notable difference to calbindin D_{9k}, where the first Ca^{2+}-binding loop is more ordered than the second on the ps-ns time-scale (Skelton et al., 1995).

The dimer interface of the structure is mainly formed by the arrangement of helices I, I′, IV and IV′. The antiparallel alignment of helices I and I′ with respect to each other is evident from the large number of NOEs between these two helices. A number of contacts are found between Pro4, Leu5 and Leu11′, Leu12′ and Ile15′ and between Ala8, Ile9 and Leu11′, Leu12′. At the helix crossover point, contacts are found from Leu11 and Leu12 to Leu11′ and Leu12′. Helices IV and IV′ are also antiparallel and aligned in a perpendicular fashion to helices I and I′, creating a scaffold arrangement. The NOEs defining the antiparallel alignment of helices IV and IV′ include Ile74 to Ile74′ (crossover point) and Phe70, Gln71, Tyr73 to Leu80′, Met82′. Leu88 is involved in the largest number of inter-molecular NOE contacts (both to helices I′ and IV′), indicating that this residue is essential for stabilizing the hydrophobic dimer interface. The perpendicular arrangement of helices I, I′ and IV, IV′, creating the scaffold, is evidenced by a substantial number of NOEs between helix I and IV′ (involving Ile13, Ile15, Phe16 and Phe70′, Tyr73′, Met82′, Asn85′). Hydrophobic interactions at the dimer interface also include inter-molecular contacts from the linker region to helix I′ (Glu41, Leu42 to Ala2, Ser3′, Ala5′, Asp6′). In a sense, the dimer interface seems to stabilize and define the linker region as well as Ca^{2+}-binding loop II.

In comparison with the previously determined structure of apo calcyclin (Potts et al., 1995), some differences should be mentioned. The most significant differences between the low- and high-resolution structures are in the packing of helices I and I′ and of helix III against helices II and IV (Table 2), as expected, within the areas of the low-resolution structure that were the least well defined. It should, however, be stressed that the observed differences are within the uncertainties of the respective structures, confirming that our earlier structure, though less precise, was none the less accurate. The changes in the structure are associated with significant differences in the experimental data. NOE contacts between helices I and I′ were not included in the previous structure calculation due to the fact that they could not be assigned from the homonuclear data alone. In contrast, NOEs between helices I and I′ could readily be identified in the heteronuclear spectra with the aid of the ^{13}C-edited, ^{13}C-filtered experiments on the mixture of labeled and unlabelled protein. Helix III is much more well defined and more closely packed against helices II and IV in the high resolution structure, with much more extensive hydrophobic interactions, in particular with the C-terminus of helix IV. This change arose because a series of NOEs were identified between Glu52, Ile53 and Lys55 in helix III and Leu80, Ile83 and Tyr84 in helix IV, as a result of the heteronuclear NMR analysis.

Discussion

Implications regarding functional properties of calcyclin

The biological importance and molecular basis for dimerization of S100 proteins has been actively debated for many years. Studies of human, mouse and rabbit calcyclin demonstrated that both covalent (cysteine disulfide) and non-covalent dimers can be formed (Ando et al., 1992; Wojda and Kuznicki, 1994). Studies by Weber and co-workers by capillary zone electrophoresis have shown that the affinity of the two subunits of S100B(ββ) for each other is at least nanomolar (Drohat et al., 1997). The low-resolution structure of apo calcyclin showed that the hydrophobic nature of the calcyclin subunit fold provides a strong driving force for the formation of non-covalent dimers.

Inspection of the high-resolution apo calcyclin structure reveals important insights into formation of covalent disulfide-linked dimers. Cys3-Cys3 disulfide dimerization in the human and mouse protein has been well characterized. Although Cys3 is substituted by Ser in rabbit calcyclin (Ando et al., 1992), we were surprised to observe that Ser3 and Ser3′ in apo calcyclin are separated by ∼20 Å. This large separation is inconsistent with formation of covalent dimers via disulfide bond formation within a single calcyclin dimer. We propose that such disulfides can only form between separate non-covalent dimers. This proposal is consistent with the rather slow rate of oxidation of the reduced calcyclin protein, and also explains why ^{1}H NMR chemical shifts do not change much upon oxidation of either human or mouse calcyclin (O. Crescenzi, S. Parikh, M.J. Lubienski and W.J. Chazin, unpublished results).

In addition to binding calcium, calcyclin has been reported to bind zinc ions (Filipek et al., 1990; Kordowska et al., 1998). Other S100 proteins have also been shown to bind zinc. It has been suggested that zinc ions bind to sites distinct from the Ca^{2+} sites. For example, in calcyclin, tyrosine fluorescence is affected in a unique manner by the binding of Zn^{2+}, and the Ca^{2+}-induced change in tyrosine fluorescence is altered by Zn^{2+}-binding (Filipek et al., 1990). This suggests that the Ca^{2+}- and Zn^{2+}-binding sites, though independent, do interact. Rabbit calcyclin contains two His residues per monomer subunit (His17 and His27), but no cysteines. The two histidines in the structure of the apo state are located very close to each other (within 8 Å), and are extremely well positioned for chelating a Zn^{2+} ion. His27, located in the first calcium-binding loop, provides a potential link between the Ca^{2+}- and Zn^{2+}-coordinating sites, which would explain the effect of Zn^{2+}-binding on the Ca^{2+}-induced effects on Tyr fluorescence. Interestingly, it is not necessary to invoke a significant change in protein conformation for there to be a Zn^{2+} effect on Ca^{2+}-induced fluorescence. His17 is close enough to Tyr19 that its effect on fluorescence could be purely electrostatic in nature. This explanation would be consistent with our preliminary NMR experiments on Ca^{2+}-loaded calcyclin, which show little change in NMR spectra upon addition of Zn^{2+} ions (M. Sastry and W.J. Chazin, unpublished results). The apo calcyclin structure readily reveals binding sites for two Zn^{2+} ions, one in each subunit. It has however been reported that human and mouse calcyclin bind four Zn^{2+} ions per dimer, and that Cys3, the only Cys residue in both molecules, is involved as a ligand for at least one of the sites (Kordowska et al., 1998). The Ser3 homolog in the apo rabbit calcyclin structure is situated at the opposite end of the molecule from the paired His residues, and must therefore participate in a different Zn^{2+}-binding site. There is no indication from the structure as to what the other ligands in this site might be.

Comparisons with other S100 apo structures

Distance differences as well as inter-residue contact analyses were performed in order to compare the apo calcyclin structure with other S100 protein structures. As discussed elsewhere (Nelson and Chazin, 1998), these approaches provide a more accurate and reliable measure of differences in protein structures than the usual methods of rmsd calculations, which are highly dependent on the atoms selected to perform superposition. Distance differences for apo calcyclin, apo rat S100B (Drohat et al., 1996) and apo bovine S100B (Kilby et al., 1996) were calculated, focusing on interfaces between individual helices to clearly identify the significant structural similarities and differences. The distance differences for calcyclin versus rat S100B, calcyclin versus bovine S100B and rat versus bovine S100B dimer subunits are displayed in Figure 5, filtered for differences larger than |3| Å. The most striking feature of the DDM results is that there are very few differences among the structures except in the packing of helix III. This is also reflected in the rather similar inter-helical angles for the I/II, I/IV

Table 2. Inter-helical angles for calcyclin, calbindin D_{9k} and S100B[a]

Helices[b]	Calcyclin	Calcyclin[c]	S100B[d]	S100B[e]	Calbindin D_{9k}
I-II	126 ± 2	129 ± 11	135 ± 3	129 ± 3	119 ± 3
I-III	-52 ± 2	-83 ± 18	-22 ± 2	-60 ± 4	-113 ± 3
I-IV	115 ± 1	119 ± 13	121 ± 2	116 ± 3	124 ± 3
II-III	-164 ± 2	146 ± 14	-138 ± 4	147 ± 4	123 ± 6
II-IV	-45 ± 1	-24 ± 9	-36 ± 2	-45 ± 4	-36 ± 5
III-IV	150 ± 2	146 ± 14	-140 ± 2	167 ± 6	121 ± 7
I-I′	-144 ± 1	-116 ± 14	-160 ± 2	-147 ± 4	–
I-IV′	-76 ± 1	-78 ± 10	-63 ± 2	-71 ± 3	–
IV-IV′	148 ± 1	148 ± 6	161 ± 2	157 ± 6	–

[a]Inter-helical angles were calculated using software written by S.M. Gagné (University of Alberta, Edmonton, AB). The signs of the angles were defined as in Drohat et al. (1996). The coordinates for apo calcyclin (1CNP), S100B(ββ) (1SYM), S100B(ββ) (1CFP) and calbindin D_{9k} (1CLB) were obtained from the Brookhaven PDB.
[b]The helices in calcyclin, S100B(ββ) and calbindin D_{9k} are defined as follows: I (4–18, 2–18, 3–14); II (31–41, 30–41, 24–35); III (50–62, 50–61, 46–54); IV (70–84, 70–83, 63–74).
[c]Refers to the structure determined by Potts et al. (1995).
[d]Rat S100B(ββ) (Drohat et al., 1996).
[e]Bovine S100B(ββ) (Kilby et al., 1996).

and II/IV helix interfaces, yet different angles for the helical pairs involving helix III (Table 2).

Distance differences were also examined for the dimer interface, including the interfaces between helices I, I′, IV and IV′. The three structures were found to be similar in all of these dimer interfaces, with no distance difference greater than 6 Å. The differences between the interfaces in the rat and bovine S100B structures were found to be comparable to those between calcyclin and the two S100B structures. Since the distance differences for the dimer interface are smaller than for the helix interfaces within the dimer subunits, any significant structural differences between calcyclin and the S100B proteins are due to differences within the subunit.

The apo calcyclin structure differs from both of the S100B structures in several ways. The largest sequence variations between calcyclin and S100B are concentrated in the linker region, the N-terminus of helix III and in helix IV. It is therefore reasonable to expect some structural differences in these regions. The linker region is relatively poorly defined in all three structures, so it is difficult to draw firm conclusions about the effect of differences in sequence. However, it is clear that the interface between helices II and III, linked by this loop, is more open in both S100B structures than in calcyclin. The linker in S100B is two residues longer than in calcyclin, and could contribute to structural differences in the II/III helix interface. The helices are better defined than the linker, and therefore any differences in these structural elements can conceivably be better correlated with sequence differences.

The ensemble of results from the various comparative analyses shows that the most significant differences among these three structures are in the relative positioning of helix III. This can readily be seen in Figure 6, which shows ribbon representations of the representative structures of the three proteins after superimposing on backbone atoms of helices I, II and IV. It is important in making such comparisons that the uncertainties in the structures are taken into account. In the ensembles representing the three structures being compared here, the rmsd from the mean of helix III is 0.53 Å (calcyclin), 0.54 Å (rat S100B) and 1.06 Å (bovine S100B). Helix III is clearly less well defined in the bovine S100B structure than in the other structures. The average pairwise backbone rmsd of helix III between the various structures has been determined over all members of each ensemble: 5.5 ± 0.2 Å (calcyclin versus rat S100B); 4.6 ± 0.4 Å (calcyclin versus bovine S100B); and 3.8 ± 0.3 Å (rat versus bovine S100B). These differences are significant because they exceed the uncertainties in the respective structures. The rsmd values indicate that each structure is unique and suggest that bovine S100B is closer to calcyclin than rat S100B. However, the rmsd value does not report on how the packing of helix III differs among the

three proteins, which is the more functionally relevant property.

The DDM (Figure 5) and inter-residue contact analyses (Table 3) provide the requisite level of detail to understand how the three structures differ. The geometry of the helix II/III interface of calcyclin is very similar to bovine S100B but different from rat S100B. This is also evident in the greater similarity of the II/III inter-helical angle for calcyclin and bovine S100B as compared to the rat S100B. Although more similar to bovine S100B, the II/III helical interface in calcyclin is clearly much more closely packed, having more than twice the number of inter-residue contacts. The geometry of the helix III/IV interface of calcyclin is distinct from both S100B proteins, in particular because the N-terminus of helix III is more closely-packed with helix IV. This is clearly evident in the larger number of inter-residue contacts between helix III and IV in calcyclin. The uniqueness of the helix III/IV interface is also reflected in the large variation in inter-helical angle. Overall, helix III is found to form more well-packed interfaces in calcyclin than in either of the S100B proteins.

The most striking observation from comparing these structures is in fact how different the two S100B structures are from each other, given that all but four residues in these proteins are identical. The most significant difference between the bovine and rat structures is the relative positioning of helices III and IV, which are almost inverted in the two structures, i.e. the top parts of the helices (closest to the Ca^{2+}-binding loop) are closer together in the bovine structure (Figures 5 and 6). This is reflected in the presence of four inter-residue contacts (Leu60-Phe76, Leu60-Ile80, Leu60-Thr81, Asp61-Thr81) in this region of the bovine structure, which are not present in the rat structure. A difference of this nature between such highly homologous proteins is unexpected and further motivated the determination of the structure of the third homolog, calcyclin, at high resolution. Although not nearly as similar in sequence as the two S100B proteins, we do not anticipate particularly large differences in the structures of these proteins. In considering the much larger number of important long-range and inter-subunit constraints identified in calcyclin in combination with the relatively large structural differences found between these structures and apo calcyclin, it appears that one or both of the apo S100B structures require further refinement. Based on the accumulated evidence of structures of other proteins with similar levels of sequence homology, we expect that this will lead to a much greater similarity between these two structures and the structure of apo calcyclin.

Table 3. Inter-residue contacts[a] in helix interfaces for calcyclin and S100B

Helices[b]	Calcyclin	S100B (rat)	S100B (bovine)
I, II	6	8	7
I,IV	9	11	8
II,III	12	11	5
II,IV	7	13	10
III,IV	19	12	11

[a]A contact between two residues is defined if their centers of geometries are within 8 Å of each other. The rmsd values were calculated by superimposing the backbone atoms in the helical regions of the protein.
[b]The helices for calcyclin, S100β are defined as follows: I (4–18, 2–18); II (31–41, 30–41); III (50–62, 50–61); IV (70–84, 70–83).

Concluding remarks

S100 proteins are purported to serve as Ca^{2+} sensor proteins that respond to the 100-fold changes in intracellular Ca^{2+} levels upon generation of Ca^{2+} signals. Since the Ca^{2+}-induced structural changes in these proteins seem to be small (Drohat et al., 1998; Sastry et al., 1998; Smith and Shaw, 1998), it is necessary to obtain structures with high precision and accuracy in order to understand how these changes lead to binding to target proteins. To this end, we have determined the three-dimensional solution structure of apo rabbit lung calcyclin with high quality and precision based on a large number of experimental constraints. The comparison to two solution structures of the homologous S100B proteins suggests that additional experimental constraints and further refinement would likely lead to some alteration in the packing of helix III. This would be important because major shifts in the packing of helix III are identified as the major structural change induced by Ca^{2+}-binding and the critical molecular basis for signal transduction. The generation of a high-resolution solution structure for the Ca^{2+}-bound state of rabbit calcyclin will enable a precise description of the molecular basis for Ca^{2+} activation and such studies are currently underway in this laboratory.

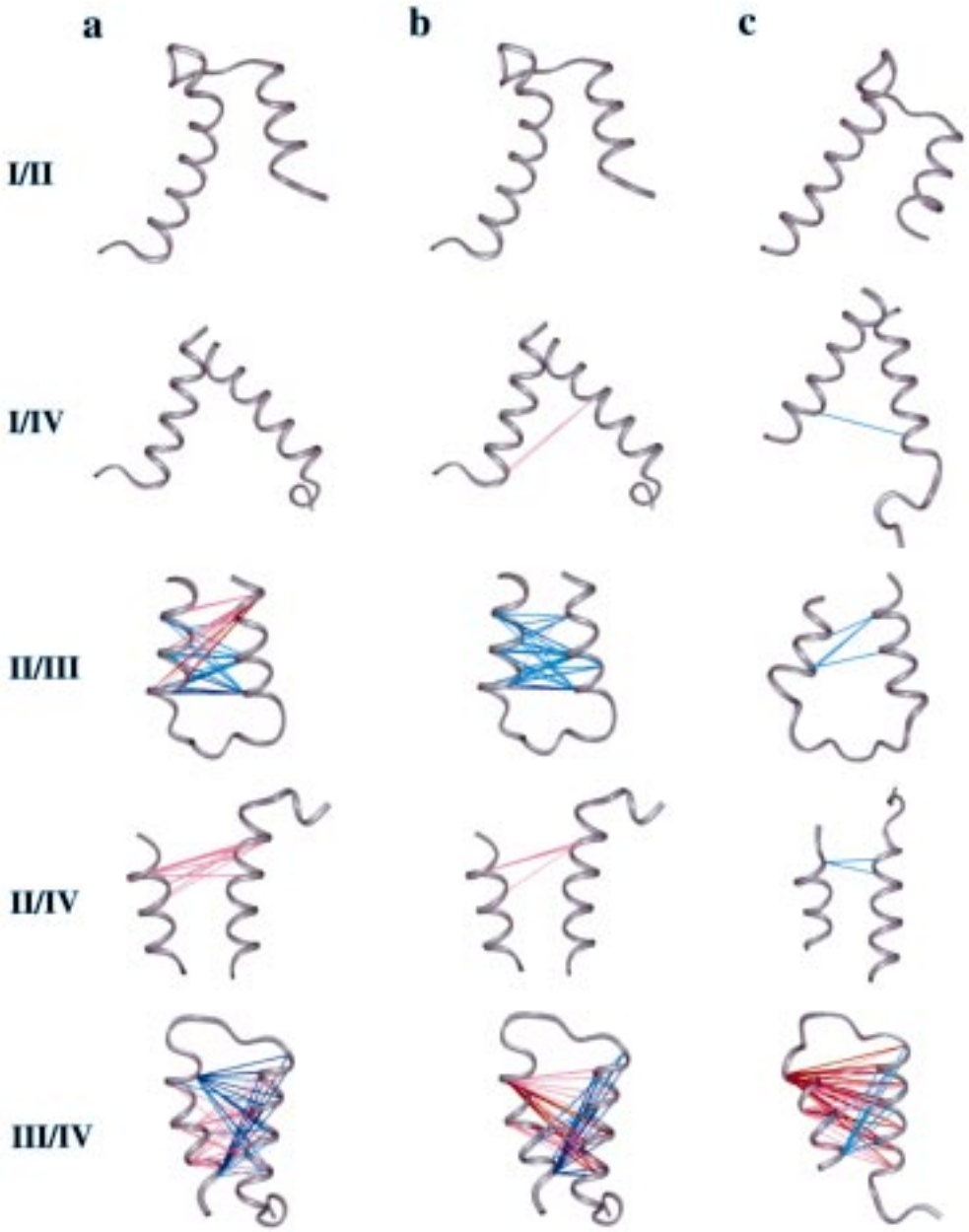

Figure 5. Distance differences calculated for the dimer subunits of apo calcyclin, apo rat S100B and apo bovine S100B. (a) Calcyclin–S100B (rat); (b) calcyclin–S100B (bovine); (c) rat S100B–bovine S100B. Negative distance differences are blue ($d \leq -5$ Å light blue, $d > -5$ Å dark blue) and positive distance differences are red ($d \leq 5$ Å light red, $d > 5$ Å dark red). Negative distances mean shorter distances in calcyclin (a, b) and in rat S100B (c). For clarity only distance differences $d > |3$ Å$|$ are displayed. Differences from calcyclin are displayed on the calcyclin structure and the differences between the rat and bovine structure are displayed on the rat S100B structure. The ribbon diagrams are shown for the structure closest to the mean of the corresponding ensemble.

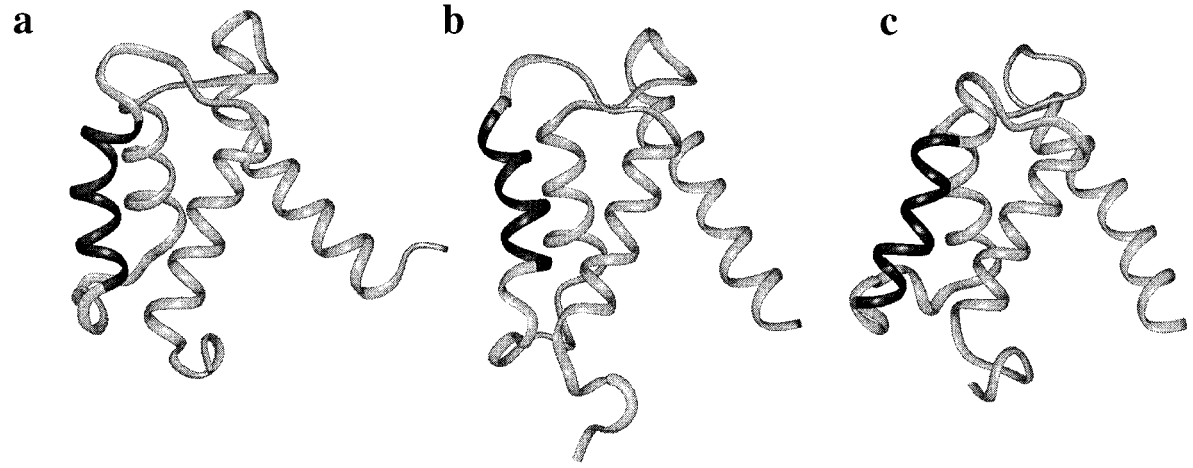

Figure 6. Structures of apo calcyclin (a), rat S100B (b) and bovine S100B (c). The figure was created by superimposing helices I and IV in all three structures, with helix III highlighted. Ribbon diagrams are shown for the structures closest to the mean.

Acknowledgements

We thank Dr. Garry Gippert for providing GENXPK and the GAP software tools, Melanie R. Nelson for providing software to analyze distance differences, Dr. Randal R. Ketchem for programs to assist NOE cross-peak assignments, Drs. Michael Lubienski and Mallika Sastry for the preparation of labeled protein, and Drs. David J. Weber, Gary S. Shaw and Mallika Sastry for helpful discussions. This research was supported by a grant from the National Institutes of Health (PO1 GM48495). L.M. acknowledges a post-doctoral fellowship from the Swedish Natural Science Research Council. W.J.C. is a Faculty Research Fellow of the American Cancer Society (FRA-436).

Note added in proof

The structure of apo rat S100B has been re-examined and further refined (A.C. Drohat, N. Tjandra, D.M. Baldisseri and D.J. Weber, *Protein Sci.*, in press). Consistent with our expectations, the revised S100B structure is much more similar to the structure of apo calcyclin than either of the earlier S100B structures.

References

Ando, Y., Watanabe, M., Akatsuka, H., Tokomitsu, H. and Hidaka, H. (1992) *FEBS Lett.*, **314**, 109–113.

Brodersen, D.E., Etzerodt, M., Madsen, P., Celis, J.E., Thøgersen, H.C., Nyborg, J. and Kjeldgaard, M. (1998) *Structure*, **6**, 477–489.

Brun, J.G., Jonsson, R. and Haga, H.J. (1994) *J. Rheumatol.*, **21**, 733–738.

Calabretta, B., Kaczmarek, L., Mars, W., Ochoa, D., Gibson, C., Hirschhorn, R. and Baserga, R. (1985) *Proc. Natl. Acad. Sci. USA*, **82**, 4463–4467.

Calabretta, B., Venturelli, D., Kaczmarek, L., Narni, F., Talpaz, M., Anderson, B., Beran, M. and Baserga, R. (1986) *Proc. Natl. Acad. Sci. USA*, **83**, 1495–1498.

Cavanagh, J., Fairbrother, W.J., Palmer III, A.G. and Skelton, N.J. (1996) Protein NMR Spectroscopy–Principles and Practice, Academic Press, San Diego, CA.

Donato, R. (1991) *Cell Calcium*, **12**, 713–726.

Drohat, A.C., Amburgey, J.C., Abildgaard, F., Starich, M.R., Baldisseri, D. and Weber, D.J. (1996) *Biochemistry*, **35**, 11577–11588.

Drohat, A.C., Baldisseri, D.M., Rustandi, R.R. and Weber, D.J. (1998) *Biochemistry*, **37**, 2729–2740.

Drohat, A.C., Nenortas, E., Beckett, D. and Weber, D.J. (1997) *Protein Sci.*, **6**, 1577–1582.

Engelkamp, D., Schäfer, B.W., Mattei, M.G., Erne, P. and Heizmann, C.W. (1993) *Proc. Natl. Acad. Sci. USA*, **90**, 6547–6551.

Filipek, A., Heizmann, C. W. and Kuznicki, J. (1990) *FEBS Lett.*, **264**, 263–266.

Filipek, A. and Kuznicki, J. (1998) *J. Neurochem.*, **70**, 1793–1798.

Gippert, G. (1995) Ph.D. Thesis, The Scripps Research Institute, La Jolla, CA.

Grzesiek, S., Kuboniwa, H., Hinck, A.P. and Bax, A. (1995) *J. Am. Chem. Soc.*, **117**, 5312–5315.

Güntert, P., Braun, W. and Wüthrich, K. (1991) *J. Mol. Biol.*, **217**, 517–530.

Güntert, P. and Wüthrich, K. (1991) *J. Biomol. NMR*, **1**, 447–456.

Ilg, E.C., Schäfer, B.W. and Heizmann, C.W. (1996) *Int. J. Cancer*, **68**, 325–332.

Jeener, J., Meier, B.H., Bachmann, P. and Ernst, R.R. (1979) *J. Chem. Phys.*, **71**, 4546–4553.

Kilby, P.M., Van Eldik, L.J. and Roberts, G.C.K. (1996) *Structure*, **4**, 1041–1052.

Kline, A.D., Braun, W. and Wüthrich, K. (1988) *J. Mol. Biol.*, **204**, 675–724.

Kördel, J., Skelton, N.J., Akke, M. and Chazin, W.J. (1993) *J. Mol. Biol.*, **231**, 711–734.

Kordowska, J., Stafford, W.F. and Wang, A.C.-L. (1998) *Eur. J. Biochem.*, **253**, 57–66.
Laskowski, R.A., MacArthur, M.W., Moss, D.S. and Thornton, J.M. (1993) *J. Appl. Crystallogr.*, **26**, 283–291.
Lee, W., Revington, M.J., Arrowsmith, C. and Kay, L.E. (1994) *FEBS Lett.*, **350**, 87–90.
Macke, T.J. (1996) Ph.D. Thesis, The Scripps Research Institute, La Jolla, CA.
Marion, D., Ikura, M., Tschudin, R. and Bax, A. (1989a) *J. Magn. Reson.*, **85**, 393–399.
Marion, D., Driscoll, P.C., Kay, L.E., Wingfield, P.T., Bax, A., Gronenborn, A.M. and Clore, G.M. (1989b) *Biochemistry*, **28**, 6150–6156.
Matsumura, H., Shiba, T., Inoue, T., Harada, S. and Kai, Y. (1998) *Structure*, **6**, 233–241.
Minami, H., Tokumitsu, H., Mizutani, A., Watanabe, Y., Watanabe, M. and Hidaka, H. (1992) *FEBS Lett.*, **305**, 217–219.
Murphy, L.C., Murphy, L.J., Tsuyuki, D., Duckworth, M.L. and Shiu, R.P.C. (1988) *J. Biol. Chem.*, **263**, 2397–2401.
Nelson, M. and Chazin, W.J. (1998) *Protein Sci.*, **7**, 270–282.
Pearlman, D.A., Case, D.A., Caldwell, J.W., Ross, W.S., Cheatham III, T.E., Ferguson, D.M., Seibel, G.L., Singh, U.C., Weiner, P.K. and Kollman, P.A. (1995) AMBER 4.1, University of California, San Francisco, CA.
Potts, B.C., Carlström, G., Okazaki, K., Hidaka, H. and Chazin, W.J. (1996) *Protein Sci.*, **5**, 2162–2174.
Potts, B.C., Smith, J., Akke, M., Macke, T.J., Okazaki, K., Hidaka, H., Case, D.A. and Chazin, W.J. (1995) *Nat. Struct. Biol.*, **2**, 790–796.
Roth, J., Teigelkamp, S., Wilke, M., Grün, L., Tümmler, B. and Sorg, C. (1992) *Immunology*, **186**, 304–314.
Sastry, M., Ketchem, R.R. Crescenzi, O., Weber, C., Lubienski, M.J., Hidaka, H. and Chazin, W.J. (1998) *Structure*, **6**, 223–231.
Schäfer, B.W. and Heizmann, C.W. (1996) *Trends Biochem. Sci.*, **21**, 134–140.
Senn, H., Messerle, W.B.A., Weber, C., Traber, R. and Wüthrich, K. (1989) *FEBS Lett.*, **249**, 113–118.
Smith, J.A., Gomez-Paloma, L., Case, D.A. and Chazin, W.J. (1996) *Magn. Reson. Chem.*, **34**, 147–155.
Smith, S.P. and Shaw, G.S. (1998) *Structure*, **6**, 211–222.
van Heyningen, V., Hayward, C., Fletcher, J. and McAuley, C. (1985) *Nature*, **315**, 513–515.
Vuister, G.W. and Bax, A. (1993) *J. Am. Chem. Soc.*, **115**, 7772–7777.
Vuister, G.W., Clore, G.M., Gronenborn, A.M., Powers, R., Garrett, D.S., Tschudin, R. and Bax, A. (1993) *J. Magn. Reson.*, **B101**, 210–213.
Wojda, U. and Kuznicki, J. (1994) *Biochem. Biophys. Acta*, **1209**, 248–252.
Wüthrich, K., Billeter, M. and Braun, W. (1983) *J. Mol. Biol.*, **169**, 949–961.
Zeng, F.-Y. and Gabius, H.-J. (1991) *Arch. Biochem. Biophys.*, **289**, 137–144.
Zeng, F.-Y., Gerke, V. and Gabius, H.-J. (1993) *Int. J. Biochem.*, **25**, 1019–1027.